^{13}C Solid-State NMR Study of Differently Processed Poly(ethylene terephthalate) Yarns

W. Gabriëlse and H. Angad Gaur

Akzo Nobel Central Research, Location Arnhem, P.O. Box 9300, 6800 SB Arnhem, The Netherlands

F. C. Feyen and W. S. Veeman*

Department of Physical Chemistry, University of Duisburg, 47048 Duisburg, Germany

Received February 18, 1994; Revised Manuscript Received June 20, 1994®

ABSTRACT: A series of fibers of poly(ethylene terephthalate) with different physical structures, varying from amorphous to 36% crystalline, has been investigated by ^{13}C solid-state NMR measurements. Several relaxation times, i.e., relaxation times in the rotating frame ($T_{1\rho}(^1H)$, $T_{1\rho}(^{13}C)$) and ^1H–^{13}C cross-polarization transfer times (T_{CH}), have been studied. ^{13}C CP/MAS spectra show that, especially with respect to the ethylene and carbonyl carbons, the chemical shift for carbons in ordered structural surroundings ("NMR crystalline") is higher than that for carbons in unordered surroundings ("NMR amorphous"). Also the width of the distribution of chemical shifts in an ordered structure is smaller than that in a less ordered structure (narrow vs broad resonance line). Analysis of the line-shape changes during the $T_{1\rho}(^{13}C)$ relaxation process of semicrystalline yarns showed that the NMR amorphous phase relaxes with two time constants. A three-region model composed of NMR crystalline, rigid NMR amorphous, and mobile NMR amorphous regions is proposed. The sizes of the rigid domains in semicrystalline PET yarns estimated from $T_{1\rho}(^1H)$ measurements correspond well with the crystal sizes as determined with X-ray diffraction. In a yarn, which is almost completely amorphous according to X-ray measurements, fast and slow ethylene and aromatic group motions, relative to a correlation time of 5×10^{-6} s, occur. From $T_{1\rho}(^1H)$ experiments it can be concluded that both mobile and rigid regions in the amorphous yarn have dimensions smaller than 50 Å. T_{CH} measurements reveal that ethylene and aromatic groups in the mobile amorphous domains of all yarns undergo large-amplitude motions. The principal elements of the chemical shift tensor of aromatic carbons remain independent of temperature up to at least 327 K, indicating that, in crystalline regions in semicrystalline yarns and in rigid parts of the amorphous yarn, phenyl reorientations have a very small amplitude (not exceeding ~5°).

Introduction

Depending on the process conditions, as-spun fibers of poly(ethylene terephthalate) (PET) exhibit quite a different physical structure. Important process parameters are the winding speed, the spinning temperature, and the viscosity of the polymers.[1,2,12] As a result of the spinning process, most of the polymer molecules are oriented along the fiber axis. In regions where polymer molecules are perfectly oriented along this axis, crystals will be formed. The degree of orientation is highly influenced by the winding speed. As-spun fibers wound at relatively low speeds are amorphous, whereas those spun at high speeds contain well-developed crystals. The yarns, drawn to an elongation at break of 10%, are well crystallized. These crystals have dimensions extending up to 100 Å along the fiber axis. A simple two-phase model, in which ordered (crystalline) regions alternate with less-ordered (amorphous) domains, has already shown to give a quite good physical description of the mechanical properties of oriented PET fibers.[1,2,18] But within this model molecular motions do not play a role. These motions, however, strongly influence the macroscopic mechanical properties of solid polymers.[3] Especially NMR relaxation measurements have proved to be very useful in the investigation of molecular motions in solid polymers.[4–6] Therefore, a variety of NMR studies has been performed on PET powders, films, and fibers.[5–8,21] A short survey of the results of previous studies will be provided first.

Sefcik et al.[5] studied quenched and annealed PET films with different crystallinities varying from 3 to 50%. They measured rotating-frame relaxation times of protons and carbons, $T_{1\rho}(^1H)$ and $T_{1\rho}(^{13}C)$. These parameters give information about molecular motions in the tens or hundreds of kilohertz range, which is a characteristic frequency range for many important motional processes in solid polymers.[4] These authors were particularly interested in $T_{1\rho}(^{13}C)$ relaxation times, which in principle can provide information about molecular motions at specific sites within the polymer. A multiexponential behavior of the ^{13}C magnetization decay was observed, but only the initial slope of the ^{13}C magnetization decay, which was used as a kind of average $T_{1\rho}(^{13}C)$ relaxation time, $\langle T_{1\rho}(^{13}C)\rangle$, was measured. As a consequence, no selective information about molecular motions in amorphous or crystalline regions was obtained directly from their relaxation measurements.

English[6] has studied PET fibers, films, and powders by various ^1H and ^{13}C solid-state NMR measurements at different temperatures. The oriented PET fibers were either almost completely amorphous (4% crystalline) or semicrystalline (49% crystalline). Attempts were made to obtain information about molecular motions by measuring proton T_1 an $T_{1\rho}$ relaxation times at different temperatures. However, in contrast to Sefcik et al.,[5] $T_{1\rho}(^1H)$ parameters were not determined from the initial decay but from the long-time limiting slope of the multiexponential ^1H magnetization decay, ignoring the 10–30% component relaxing more rapidly. So again, the multiexponential behavior was not interpreted in terms of different types of molecular motions within the polymer.

Cheung et al.[8] have also performed $T_{1\rho}(^1H)$ measurements on 50% crystalline PET films. They observed two distinct $T_{1\rho}(^1H)$'s that were assigned to different phases within the sample with different motional character. However, proton spin diffusion often plays an important

® Abstract published in *Advance ACS Abstracts*, August 1, 1994.

0024-9297/94/2227-5811$04.50/0

Table 1. Crystallinity (V_C), Amorphous Orientation (F_{aa}), and Amorphous Orientation Distribution (F_{aa}/F_{ab}) Data of the Series of PET Yarns

sample	V_C	F_{aa}	F_{aa}/F_{ab}
1. 5500(10%)	0.367	0.799	1.38
2. 500(10%)	0.352	0.821	1.19
3. 5500	0.239	0.652	2.35
4. 4200	0.116	0.470	2.13
5. 500	0.01	0.008	1.83

role in $T_{1\rho}(^1H)$ measurements, which can result in the averaging of intrinsic relaxation times[14-16,19] corresponding to different regions within the sample. So the two observed $T_{1\rho}(^1H)$'s do not necessarily correspond to two distinct regions within the sample but can reflect more than two regions. Indeed, Havens et al.[7] also observed two $T_{1\rho}(^1H)$'s for various PET samples, but three components were obtained from their spin diffusion experiments. They found the two-phase amorphous/crystalline model to be a poor representation of semicrystalline PET yarns and proposed a three-domain structure composed of crystalline, rigid amorphous, and mobile amorphous domains.

In this paper, we report an NMR study of a series of both as-spun (wound at different winding speeds of 500–5500 m/min) and drawn PET yarns (to an elongation at break of 10%). Two rotating-frame relaxation parameters, $T_{1\rho}(^1H)$ and $T_{1\rho}(^{13}C)$, and the ^1H–^{13}C cross-polarization transfer time, T_{CH}, were studied. In interpreting our relaxation measurements, the full relaxation curves were analyzed. In addition, we made use of differences in chemical shift and line width between ordered and disordered domains as they appear in carbonyl and ethylene resonances in ^{13}C CP/MAS spectra. Combination of relaxation data with line-shape information provides detailed insight into both physical structure and molecular motion of PET yarns with different processing histories. Information about the amplitude of aromatic ring motions is obtained by measuring the principal elements of the chemical shift tensor of aromatic carbons at different temperatures. In this study, we compare NMR relaxation parameters of the different samples and relate them to data obtained by X-ray diffraction, density, and sonic pulse propagation measurements.[1,2,18]

Experimental Section

Samples. Five PET fibers were spun at different winding speeds of 500, 4200, and 5500 m/min. Two samples, originally spun at 500 and 5500 m/min, were additionally drawn to an elongation at break of 10%. The spinning temperature was 290 °C, and the diameter of the capillaries was 500 μm. The relative viscosity[18] of the polymers was 1.82. Other structure parameters of the samples studied are given in Table 1. We will only give a brief qualitative explanation of these quantities. More detailed information has been given elsewhere.[1,2,18] The samples are denoted by their winding speed.

The volume fraction crystalline material, V_C, varies between 0.01 for an undrawn slow-spun yarn (500 m/min) and 0.367 for a fast-spun drawn yarn (5500 m/min). These values are determined by a combination of X-ray diffraction and density measurements.[18] As a measure of the level of chain orientation in the amorphous phase, the factor based on sonic modulus measurements, F_{aa}, has been chosen. This value can vary theoretically from zero for unoriented to 1 for perfectly oriented systems. Birefringence measurements have also been used to determine the amorphous orientation, indicated by F_{ab} values. The ratio F_{aa}/F_{ab}, given in Table 1, was previously found to be a good representation of the width of the orientation distribution in the amorphous phase which should be related, at least qualitatively, to the contour-length distribution.[18] This value varies in this series between 1.19 for narrow distributions and 2.35 for the broadest.

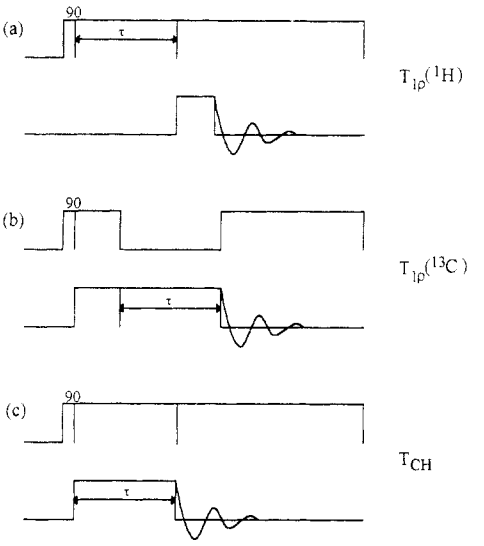

Figure 1. Schematic representation of pulse sequences used: (a) $T_{1\rho}(^1H)$ experiment; (b) $T_{1\rho}(^{13}C)$ experiment; (c) variable cross-polarization contact-time experiment for determining T_{CH} parameters.

NMR Spectroscopy. NMR measurements were performed on a Bruker MSL400 spectrometer operating at 400 MHz for ^1H. In all measurements cross-polarization (CP) techniques and proton-decoupling were combined with magic-angle spinning (MAS) in order to obtain high-resolution ^{13}C spectra. A double-bearing CP/MAS probe was used with 4-mm spinners. For the $T_{1\rho}(^{13}C)$ experiments the spinning frequency was 9 kHz. All other experiments were performed at a rotor speed of 4.6 kHz. At these spinning frequencies overlapping of resonances at isotropic positions with spinning sidebands did not occur. Two radio-frequency field strengths of 44 and 78 kHz were used for protons and carbons. The recycle delay was 8 s. Phase cycling and spin temperature alternation were used to minimize artifacts.[10] Adamantane was used to optimize the Hartmann–Hahn condition for cross-polarization and as an external secondary chemical shift reference (38.56 ppm for the methylene resonance relative to TMS).

The pulse scheme for measuring $T_{1\rho}(^1H)$ values is given in Figure 1a. ^{13}C relaxation times in the rotating frame, $T_{1\rho}(^{13}C)$, were measured with the pulse sequence of Figure 1b. The CP contact time is 2 ms. Both relaxation parameters are obtained by fitting the measured intensities, $M(\tau)$, to one or to a sum of exponentials:

$$M(\tau) = \sum_i M_{0i}\, e^{-\tau/T_{1\rho i}} \tag{1}$$

^1H–^{13}C cross-polarization times, T_{CH}, were determined in a variable contact-time CP/MAS experiment (see Figure 1c). T_{CH} values were obtained by fitting $M(\tau)$ to:[11]

$$M(\tau) = \sum_i M_{0i}\left[\frac{e^{-\tau/T_{1\rho i}(^1H)} - e^{-\tau/T_{CH_i}}}{(1 - T_{CH_i}/T_{1\rho_i}(^1H))}\right] \tag{2}$$

Equation 2 is composed of an ascending function describing the buildup of ^{13}C magnetization with time constant T_{CH} and a descending function describing the loss of magnetization as a result of relaxation in the rotating frame with time constant $T_{1\rho}(^1H)$. In principle, this equation should also contain a $T_{1\rho}(^{13}C)$ parameter.[11] However, experimental data fitting showed that the contribution of the known $T_{1\rho}(^{13}C)$ parameter was negligible. Spectra at different τ were obtained by repeatedly cycling through the range of delay times, for each time adding at least 80 free induction decays (FIDs). This accumulation method eliminates possible experimental drift errors caused by spinner instability or by small fluctuations in spectrometer performance during the measuring time (8–64 h).

Results and Discussion

A. ^{13}C CP/MAS Spectra. Figure 2 illustrates ^{13}C CP/MAS spectra of two PET yarns. Figure 2a shows a

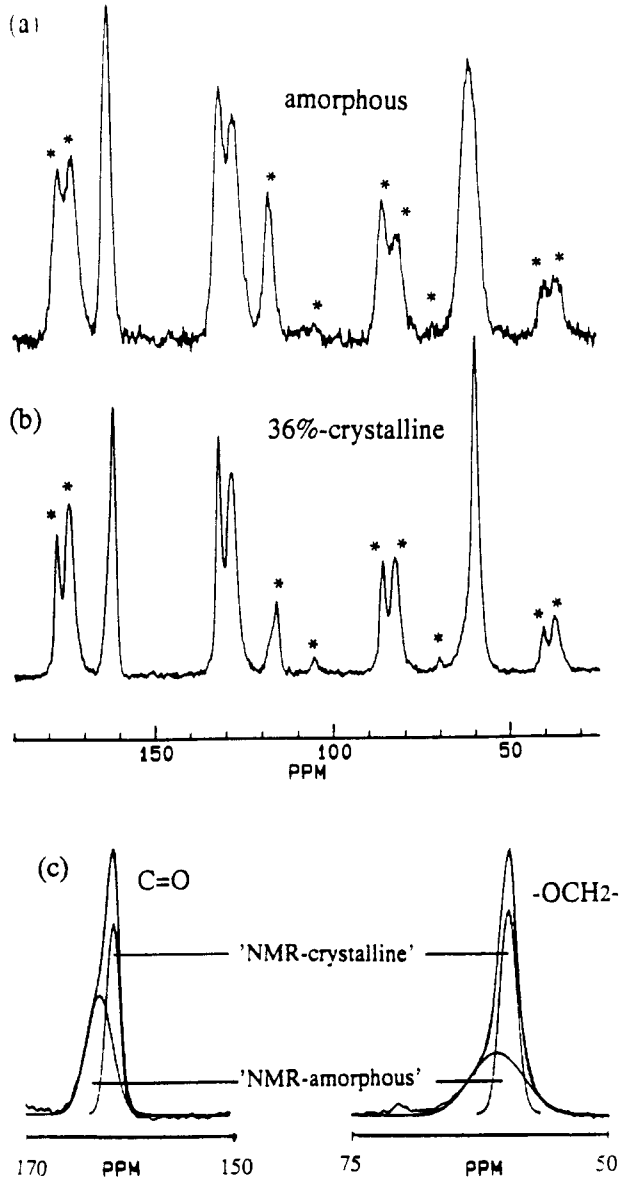

Figure 2. ^{13}C CP/MAS spectra of different PET yarns (CP-mix = 2 ms, ν_1 = 44 kHz, rotor speed = 4.6 kHz). Spinning sidebands are marked with an asterisk. No window functions were applied. Spectra a and b are obtained by accumulating 1440 and 990 FIDs, respectively. (a) Amorphous yarn (sample 500); (b) 36% crystalline yarn (sample 5500(10%)); (c) deconvolution spectra of ethylene and carbonyl resonances of Figure 2b.

Table 2. Chemical Shift (δ) Values for Ethylene, Protonated Aromatic, Nonprotonated Aromatic, and Carbonyl Carbon Resonances of a 36% Crystalline Yarn (Sample 5500(10%)) and an Amorphous Yarn (Sample 500)

	δ (ppm)	
nucleus	36% cryst.	amorphous
CH_2	62.5	63.9
protonated aromatic	131.0	130.4
nonprotonated aromatic	134.7	134.1
C=O	164.5	166.1

spectrum of an amorphous yarn wound at relatively low speed (sample 500). Figure 2b shows a spectrum of a 36% crystalline yarn wound at relatively high speed (sample 5500(10%)). Chemical shift (δ) values of different carbons are given in Table 2. The ethylene and carbonyl carbon resonances of the amorphous yarn are shifted about 1 ppm downfield with respect to the semicrystalline yarn, as opposed to the aromatic carbons which are shifted slightly unfield. Besides differences in chemical shift, the spectrum of the 36% crystalline yarn shows narrower lines with a better signal/noise ratio than the spectrum of the amorphous yarn. The broader lines in Figure 2a are attributed to a broader orientation distribution of polymer molecules, which results in a larger distribution of isotropic chemical shifts.[13] Additional differences between both spectra are observed in the line shape: the ethylene and carbonyl carbon resonances in Figure 2a have a symmetric line shape, whereas these lines in Figure 2b are asymmetric. The asymmetric line shape is resolvable into two partially overlapping resonances: a relatively broad low-field component and a relatively narrow high-field component (Figure 2c). The narrow component is shifted ~1 ppm upfield with respect to the broad component. Peak deconvolution has been performed by use of a computer simulation program distributed by Bruker (Linesim). The broad resonance line in Figure 2c corresponds both in line width and in chemical shift with the resonance lines of the amorphous yarn in Figure 2a. The broad resonance is therefore assigned to the disordered NMR amorphous phase and the narrow peak to ordered NMR crystalline regions. The asymmetric line shape of ethylene and carbonyl resonances in ^{13}C CP/MAS spectra of PET yarns has also been reported by other authors.[5,21]

B. $T_{1\rho}(^{13}C)$ Relaxation. 1. Introduction. $T_{1\rho}(^{13}C)$ parameters of different carbons are not averaged by spin diffusion, because the low natural abundance of ^{13}C spins ensures a physical separation within the solid and hence a slow or vanishingly slow ^{13}C spin diffusion rate. This makes $T_{1\rho}(^{13}C)$ parameters interesting to study, because they can provide information about molecular motions of specific sites within a polymer molecule.

However, a complexity may arise in the quantitative interpretation of $T_{1\rho}(^{13}C)$ parameters as a motional parameter.[3,4,16,20] In a $T_{1\rho}(^{13}C)$ experiment ^{13}C spins are coupled to the lattice in two ways. For both mechanisms the carbon spins are coupled to fluctuating local magnetic fields due to protons. In the first process these fluctuating fields arise from molecular motions which modulate the ^{13}C–^{1}H dipolar interaction. This constitutes the normal spin–lattice relaxation process characterized by time constant $T_{1\rho}(^{13}C)$. For the second mechanism strong ^{1}H–^{1}H dipolar interactions give rise to fast proton–proton spin flip-flops, which also modulate the ^{13}C–^{1}H dipolar coupling. This is a pure spin–spin relaxation process and can be described as a thermal contact with characteristic time T_{CH}^{D} between the ^{13}C rotating-frame Zeeman reservoir and the ^{1}H dipolar reservoir, which in turn is coupled to the lattice with time constant T_{1D}^{H}. So, $T_{1\rho}(^{13}C)$ relaxation can occur via a pathway involving motional spin–lattice processes (^{13}C rotating-frame Zeeman reservoir → lattice) and nonmotional spin–spin processes (^{13}C rotating-frame Zeeman reservoir → dipolar reservoir → lattice). It has been shown that under magic-angle spinning conditions $T_{1D}^{H} \ll T_{1\rho}(^{13}C)$, T_{CH}^{D},[16,17] so that the dipolar reservoir and the lattice can be considered as one reservoir to which the ^{13}C rotating-frame Zeeman reservoir relaxes with an effective relaxation time:

$$\frac{1}{T_{1\rho}^{*}(^{13}C)} = \frac{1}{T_{1\rho}(^{13}C)} + \frac{1}{T_{CH}^{D}} \qquad (3)$$

Spin–spin processes become especially important for rigid systems in which internuclear proton–proton and carbon–proton distances are small. In those systems motional information cannot always be retrieved from $T_{1\rho}(^{13}C)$ measurements. Schaefer et al.[3] estimated the spin–spin contribution to $T_{1\rho}(^{13}C)$ for oriented PET films at some 30–40%. Sefcik et al.[5] concluded that $T_{1\rho}(^{13}C)$

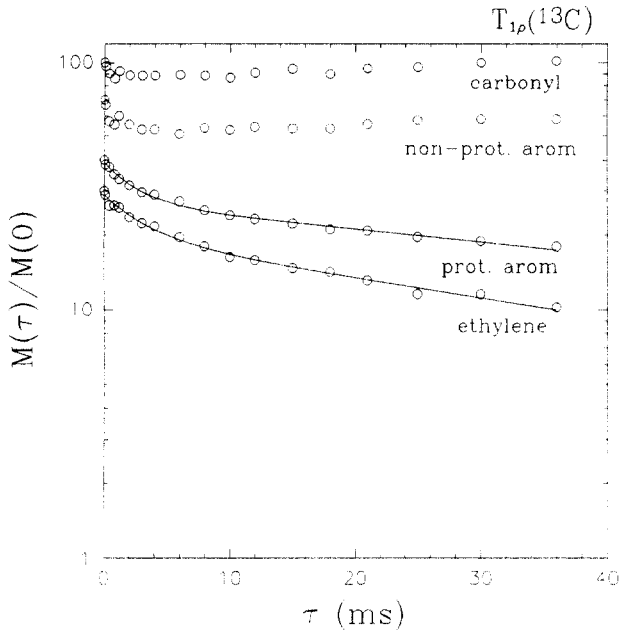

Figure 3. $T_{1\rho}(^{13}C)$ relaxation behavior (ν_1 = 78 kHz, rotor speed = 9.0 kHz) of chemically different carbons of sample 5500(10%). For the sake of visual clarity, data of different carbons are displaced vertically.

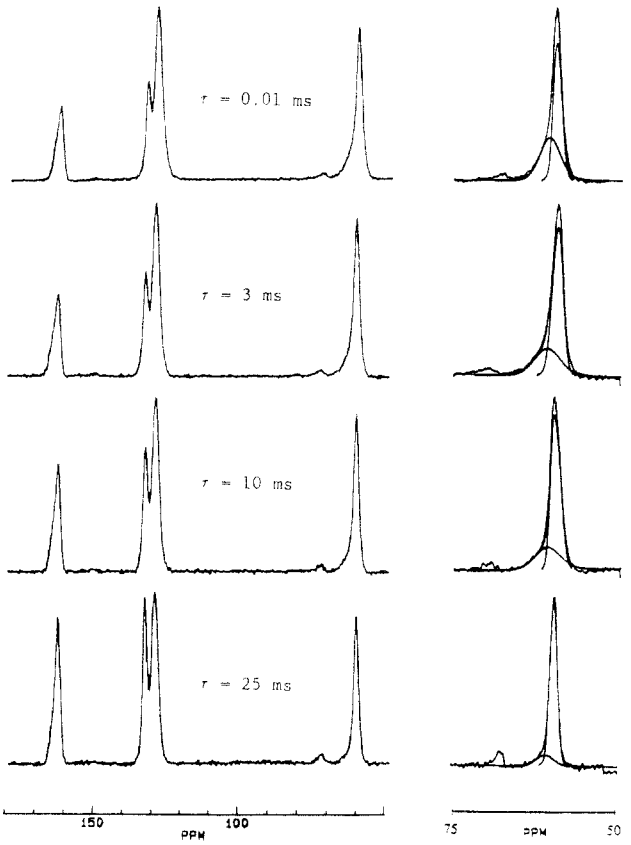

Figure 4. ^{13}C CP/MAS spectra (ν_1 = 78 kHz, rotor speed = 9 kHz) with corresponding deconvoluted spectra of ethylene resonances at different stages in the $T_{1\rho}(^{13}C)$ relaxation process for sample 5500(10%).

relaxation in crystalline regions of PET yarns is spin–spin dominated. Their conclusions were based on average $\langle T_{1\rho}(^{13}C)\rangle$ and $\langle T_{CH}{}^{D}\rangle$ measurements at relatively low ν_1 fields, ranging from 28 to 44 kHz. We will show that especially at a relatively high ν_1 field of 78 kHz, which favors spin–lattice over spin–spin contributions to $T_{1\rho}(^{13}C)$ relaxation,[16,20] $T_{1\rho}(^{13}C)$ relaxation times can be interpreted as motional parameters.

Table 3. $T_{1\rho}(^{13}C)$ Relaxation Values with Corresponding Fractions of (1) Ethylene, (2) Protonated Aromatic, (3) Nonprotonated Aromatic, and (4) Carbonyl Carbons Measured at Different ν_1 Fields (44 and 78 kHz)

sample	ν_1 (kHz)	$T_{1\rho}(^{13}C)_A$ (ms)	$T_{1\rho}(^{13}C)_B$ (ms)	I_A (%)	I_B (%)
		1. Ethylene			
1. 5500(10%)	44	0.6 ± 0.4	8.6 ± 1.2	25 ± 6.1	75 ± 6.2
	78	3.4 ± 0.7	54.0 ± 7.8	33 ± 3.8	67 ± 4.0
2. 500(10%)	44	1.4 ± 0.3	10.3 ± 1.8	50 ± 4.2	50 ± 4.4
3. 5500	44	1.4 ± 0.2	8.4 ± 1.0	54 ± 5.2	46 ± 5.4
5. 500	44	1.7 ± 0.2		100 ± 3.4	
	78	1.5 ± 0.4	21.5 ± 2.3	34 ± 4.7	66 ± 4.3
		2. Protonated Aromatic			
1. 5500(10%)	44	1.4 ± 0.3	15.1 ± 1.3	37 ± 3.9	63 ± 4.1
	78	2.6 ± 0.3	83.3 ± 8.6	32 ± 1.8	68 ± 1.8
2. 500(10%)	44	1.0 ± 0.2	13.0 ± 0.9	34 ± 3.2	66 ± 3.2
3. 5500	44	1.0 ± 0.2	12.6 ± 0.7	33 ± 2.4	67 ± 2.6
5. 500	44	0.6 ± 0.1	5.6 ± 1.0	50 ± 5.4	50 ± 5.6
	78	1.3 ± 0.2	23.2 ± 2.4	49 ± 3.1	51 ± 3.2
		3. Nonprotonated Aromatic			
1. 5500(10%)	44		92.1 ± 19		75 ± 2.5
	78		>100		
2. 500(10%)	44		101 ± 17		73 ± 2.4
3. 5500	44		65.7 ± 24		72 ± 8.0
5. 500	44		38.1 ± 4.2		71 ± 4.0
	78		46.8 ± 4.0		100 ± 1.9
		4. Carbonyl			
1. 5500(10%)	44		91.7 ± 14		81 ± 2.1
	78		>100		
2. 500(10%)	44		121 ± 30		80 ± 3.4
3. 5500	44		44.1 ± 3.4		100 ± 1.5
5. 500	44		32.9 ± 2.2		76 ± 2.2
	78		49.9 ± 1.8		100 ± 0.8

2. Results. $T_{1\rho}(^{13}C)$ Measurements. In Figure 3 the decay of ^{13}C magnetization of chemically different carbons is plotted logarithmically as a function of τ for sample 5500(10%). Solid lines represent least-squares fits to the relaxation data (open symbols) using eq 1. For the sake of visual clarity relaxation data of different carbons are displaced vertically. This plot indicates that the decay of ^{13}C magnetization of the protonated carbons involves at least two different relaxation times. For the nonprotonated carbonyl and aromatic carbons the relaxation process is more complicated and not well-understood. Due to the large C–H distance, one expects a much longer $T_{1\rho}(^{13}C)$ which is also observed. However, a sizable fraction (~25%) shows a not clearly defined fast initial decay. Because of the complex results, $T_{1\rho}(^{13}C)$ results of nonprotonated carbons are not further discussed. The other PET yarns show a comparable $T_{1\rho}(^{13}C)$ relaxation behavior. The relaxation data are summarized in Table 3. For the nonprotonated carbons only the longer $T_{1\rho}(^{13}C)$ values with their fractions are given. For two samples (500 and 5500 (10%) $T_{1\rho}(^{13}C)$ measurements were performed at different ν_1 fields (44 and 78 kHz).

It is tempting to correlate the two relaxation times of protonated carbons with the amorphous/crystalline two-phase structure. However, the various relaxation mechanisms involved in the $T_{1\rho}(^{13}C)$ relaxation process may also result in a biexponential decay. To elucidate this point, we examined ^{13}C spectra at different stages in the $T_{1\rho}(^{13}C)$ relaxation process. In Figure 4 ^{13}C CP/MAS spectra at different delay times τ (ν_1 = 78 kHz, rotor speed = 9 kHz) are shown for sample 5500–10%. From these spectra it is clear that the line widths of the ethylene, carbonyl, and aromatic resonances decrease with increasing τ. This is, for instance, clearly reflected by the better resolution between the peaks due to protonated and nonprotonated carbons. The deconvoluted spectra of the ethylene

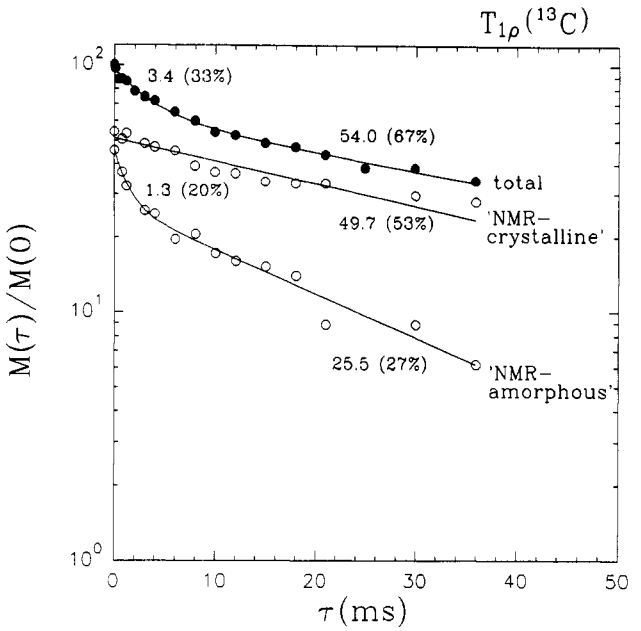

Figure 5. $T_{1\rho}(^{13}C)$ relaxation behavior of the total ethylene resonance and of the NMR crystalline and NMR amorphous components of sample 5500(10%) (ν_1 = 78 kHz, rotor speed = 9000 Hz). $T_{1\rho}(^{13}C)$ parameters (in ms) with fractions (in brackets) are given for each slope. Solid lines represent least-squares fits to the relaxation time data using eq 1.

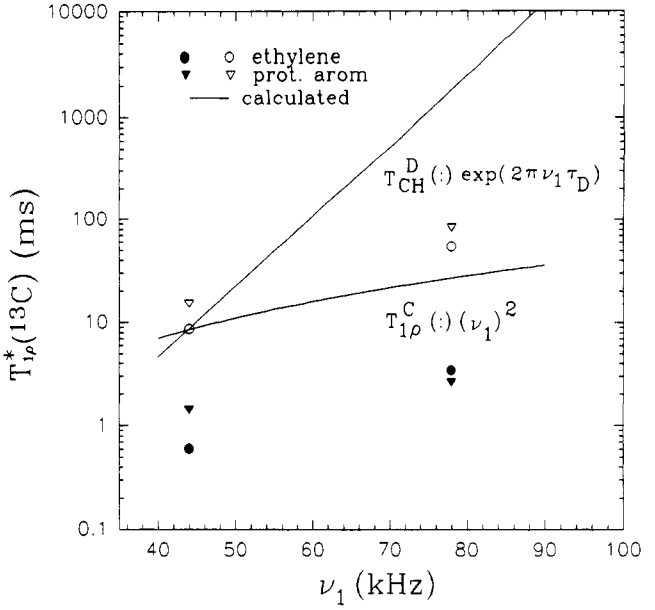

Figure 6. $T_{1\rho}(^{13}C)$ relaxation values as a function of ν_1. Symbols represent the longer $T_{1\rho}(^{13}C)_B$ values (open symbols) and shorter $T_{1\rho}(^{13}C)_A$ values (filled symbols) of ethylene and protonated aromatic carbons of sample 5500(10%) measured at 44 and 78 kHz (see Table 3). Solid lines represent calculated dependences in the case of spin–spin (T_{CH}^{D}) and spin–lattice ($T_{1\rho}(^{13}C)$ processes. Solid lines are arbitrarily scaled; τ_D was taken to be 24 μs.

resonances, shown in the same Figure, reveal that this line narrowing is due to a loss of relatively fast relaxing ^{13}C magnetization in the NMR amorphous phase. We confirmed this by measuring individually the decay of ^{13}C magnetization of the NMR amorphous and NMR crystalline components of the ethylene resonance. The results in Figure 5 indeed show that NMR amorphous regions relax at a faster rate than NMR crystalline regions. Additionaly, two $T_{1\rho}(^{13}C)$ relaxation times (1.3 and 25.5 ms) are involved in the decay of ^{13}C magnetization of the NMR amorphous phase, whereas the decay of ^{13}C magnetization in NMR crystalline regions could be fitted with one time constant (49.7 ms). So, by analyzing the line shape, we conclude that three instead of two relaxation times are involved in the relaxation process of ethylene carbons, which correspond to different regions within the sample. Although not completely analyzed, all semicrystalline yarns show a line narrowing with increasing τ in a $T_{1\rho}(^{13}C)$ experiment. It should be noted that Table 3 shows the results of a fitting procedure with only two components. So, the short relaxation time in Table 3 represents a kind of average relaxation time for the NMR amorphous phase.

With the aid of two arguments we will show that especially at high ν_1 fields the observed $T_{1\rho}(^{13}C)$ relaxation times reflect molecular motions and are not or little influenced by spin–spin processes.

(i) First, while NMR crystalline regions relax with a relaxation time of ~50 ms, T_{CH}^{D} for NMR crystalline regions must have at least this value. The NMR amorphous regions are expected to have longer T_{CH}^{D} values than the densely packed crystalline regions, so even longer than 50 ms. Because the observed $T_{1\rho}(^{13}C)$ relaxation times of NMR amorphous regions (1.3 and 25.5 ms) are significantly shorter than 50 ms, it can be concluded that molecular motions dominate the $T_{1\rho}(^{13}C)$ relaxation process in these regions. We therefore assign the short and the long $T_{1\rho}(^{13}C)$ relaxation times of the NMR amorphous phase to mobile and rigid regions, respectively, in this phase.

(ii) For the NMR crystalline relaxation time (49.7 ms), the contribution of T_{CH}^{D} can be estimated by examining the ν_1 field dependence of $T_{1\rho}(^{13}C)$ and T_{CH}^{D}.[16] In the case of spin-spin interactions, giving rise to $T_{1\rho}(^{13}C)$ relaxation, an exponential dependence of T_{CH}^{D} on ν_1 has been given.[16] Hence, T_{CH}^{D} (:) $\exp(2\pi\nu_1\tau_D)$, where τ_D represents the correlation time for proton dipolar fluctuations. The spin–lattice contribution to $T_{1\rho}(^{13}C)$ arises from time-dependent dipolar interactions between carbon and proton spins, which are time dependent because of molecular motion. When we assume that the internuclear carbon–proton vectors fluctuate by random isotropic rotational diffusion, the autocorrelation function $G(\tau)$ decays exponentially with a single rotational correlation time τ_c, and $T_{1\rho}^{C}$ will be given by:[16,20]

$$\frac{1}{T_{1\rho}^{C}} = \frac{N_H\gamma_H^2\gamma_C^2\hbar^2}{20r_{CH}^6}\left(\frac{\mu_0}{4\pi}\right)^2\left\{\frac{4\tau_C}{1+\omega_1^2\tau_c^2} + \frac{\tau_c}{1+(\omega_H-\omega_C)^2\tau_c^2} + \frac{3\tau_c}{1+\omega_C^2\tau_c^2} + \frac{6\tau_c}{1+\omega_H^2\tau_c^2} + \frac{6\tau_c}{1+(\omega_H+\omega_C)^2\tau_c^2}\right\} \quad (4)$$

where N_H is the proton natural abundance, γ is the nuclear gyromagnetic ratio, $\nu_H = \omega_H/2\pi$ and $\nu_C = \omega_C/2\pi$ are the resonance frequencies of protons and carbons, respectively, $\nu_1 = \omega_1/2\pi$ is the ^{13}C radio-frequency field strength, μ_0 the permeability constant, and r_{CH} the internuclear carbon–proton distance. For $\omega_1\tau_c \ll 1$, $T_{1\rho}(^{13}C)$ is independent of ω_1. For $\omega_1\tau_c \gg 1$, only the first term in eq 4 is important and $T_{1\rho}(^{13}C)$ (:) $(\omega_1)^2$.

It can easily be seen that the difference in ν_1 field dependence between spin–spin and spin–lattice relaxation predicts a small contribution of spin–spin processes to $T_{1\rho}(^{13}C)$ at high ν_1 fields. This has been graphically illustrated in Figure 6 where both calculated dependences (arbitrarily scaled) are given. In our calculations τ_D was taken to be 24 μs, which corresponds with the measured and calculated value for high-density linear polyethylene with strongly coupled protons as studied by VanderHart

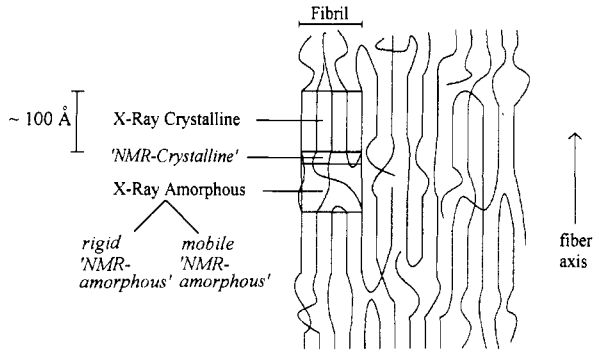

Figure 7. Schematic representation of the physical structure of semicrystalline PET yarns.

et al.[16] In PET τ_D will be longer than that in high-density polyethylene, because of weaker proton–proton interactions. Therefore, our calculations of the spin–spin relaxation process as a function of the ν_1 field describe a limiting case. A longer correlation time means a stronger field dependence and so a bigger distinction between spin–spin and spin–lattice effects. The symbols represent experimental data of the protonated carbons of sample 5500(10%) (see also Table 3). The data of sample 500, measured at different fields, are not given in the same figure but will be discussed later on. It can be seen that both the observed longer $T_{1\rho}(^{13}C)_B$ values (open symbols) and the shorter $T_{1\rho}(^{13}C)_A$ values (filled symbols) follow a nearly $(\nu_1)^2$ dependence, which indicates the contribution of molecular motion to $T_{1\rho}(^{13}C)$. The observed relaxation times at 78 kHz are a little longer than the calculated values according to a $(\nu_1)^2$ dependence (with the exception of the short relaxation time of protonated aromatic carbons discussed later on). This can be attributed to a small contribution of spin–spin processes to $T_{1\rho}(^{13}C)$ at lower fields. Hence, we expect that, at relatively high ν_1 fields of 78 kHz, $T_{1\rho}(^{13}C)$ relaxation is almost entirely due to molecular motions.

3. Physical Structure. The observation of three distinct $T_{1\rho}(^{13}C)$'s of the ethylene carbons of sample 5500 (10%) measured at 78 kHz (see Figure 5) must correspond to three different mobility regimes within the sample. Together with the line-shape information this brings us to the conclusion that we can distinguish between three regions within a semicrystalline PET fiber: NMR crystalline, rigid NMR amorphous, and mobile NMR amorphous. This is in general agreement with the results of Havens et al.,[7] who came to the same conclusion based on proton spin diffusion experiments. For the physical interpretation of these regions our starting point will be a simple description of the physical structure of drawn PET yarns as proposed by Heuvel et al.[1,2,18] A schematic picture is given in Figure 7. In this model well-ordered crystalline regions alternate with less-ordered amorphous domains. Since single chains pass from several crystalline regions into amorphous regions, coherent structural units, called fibrils, are formed.

The NMR crystalline fraction can, of course, be assigned to the well-ordered crystalline regions. However, the fraction NMR crystalline (53%) of sample 5500(10%) is significantly larger than the fraction of X-ray crystalline material (36.7%). At this point we define the notion of crystallinity. On the one hand, we measure and discuss the crystallinity determined by X-ray measurements. These fractions indicate the relative amount of crystalline regions with sizes over ~50 Å, namely, the X-ray crystallinity. On the other hand, the NMR crystallinity, based on $T_{1\rho}(^{13}C)$ measurements, relies on our experimental

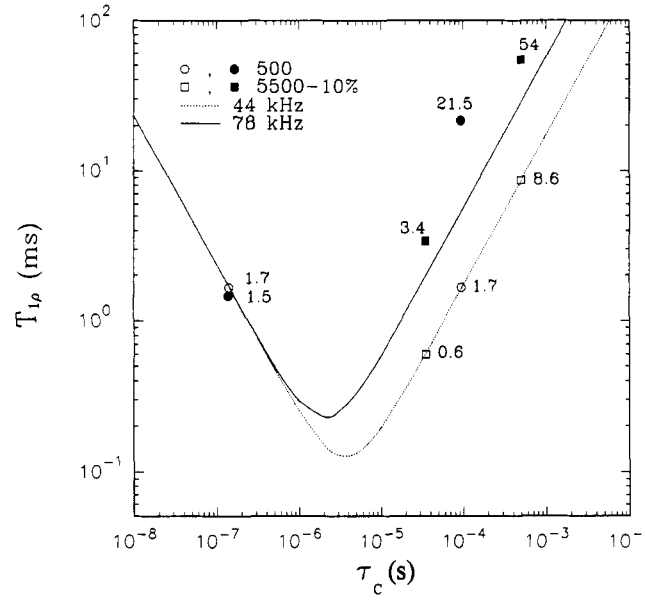

Figure 8. Calculated dependences of $T_{1\rho}(^{13}C)$ on τ_c according to eq 4 for two different ν_1 fields (ν_1 = 44 and 78 kHz). $T_{1\rho}(^{13}C)$ relaxation data of the ethylene carbons of sample 500 and 5500-(10%) measured at 44 and 78 kHz (see Table 3) are given by open and filled symbols, respectively.

findings that in PET yarns, especially with respect to the ethylene and carbonyl carbons, the chemical shift for carbons in ordered structural surroundings (NMR crystalline) is higher than that for carbons in unordered surroundings (NMR amorphous). Also the width of the distribution of chemical shifts in an ordered structure is smaller than that in an unordered structure (narrow vs broad line). Since the ^{13}C chemical shift is sensitive to its surroundings over a distance of not much more than 5 Å, small regions that may not be called crystalline from the X-ray diffraction point of view can be NMR crystalline.

The discrepancy between the X-ray crystallinity and the NMR crystallinity can now be explained in two ways. First, small crystalline regions (<~50 Å) that cannot be detected by X-ray measurements will contribute to the NMR crystalline fraction. Second, when we depart from the above-mentioned model, in which disordered amorphous domains interconnect ordered crystalline regions, it is conceivable that there will be a gradual transition from ordered to disordered polymer molecules. We could imagine that those polymer molecules that just leave or enter the crystalline regions (see Figure 7) are still ordered to a relatively high degree and have an NMR crystalline chemical shift.

In the NMR amorphous phase we distinguish between relatively fast and slow molecular motions. Since a variety of structures within the amorphous phase can be imagined, it is not possible from the present study to assign these motions to specific structural units within this phase. However, we can imagine that there exist some tie chains in the amorphous phase connecting the stiff crystalline units which are relatively rigid. On the other hand, loose chain loops or chain ends terminating in the amorphous phase, but possibly also disordered chains that are in between the more oriented fibrils, may move more freely.

4. Molecular Motions. In an attempt to explain the radio-frequency field dependence of the $T_{1\rho}(^{13}C)$ values, Figure 8 shows the calculated dependence of $T_{1\rho}(^{13}C)$ on τ_c according to eq 4 (isotropic motions) for two different ν_1 fields (44 and 78 kHz). The internuclear carbon–proton distance, r_{CH}, was taken to be 1.10 Å. This plot shows that for fast molecular motions ($\omega_1\tau_c \ll 1$), $T_{1\rho}(^{13}C)$ is inde-

pendent of ν_1, while for slow molecular motions ($\omega_1\tau_c \gg 1$), $T_{1\rho}(^{13}C)$ is longer at a higher ν_1 field (78 kHz), following a $(\nu_1)^2$ dependence. Although the assumption of random isotropic rotational diffusion is a far too simple representation of the ethylene reorientational motions, the general appearance of the dependence of $T_{1\rho}(^{13}C)$ on τ_c may be expected to be similar to the curve in Figure 8. So we use this model in a qualitative way, which appears to be helpful in interpreting the relaxation data.

The measured $T_{1\rho}(^{13}C)$ values of the ethylene carbons of sample 500 and 5500(10%) measured at 44 kHz (open symbols) and 78 kHz (filled symbols) are given in the same figure. The values measured at 78 kHz are plotted against the same τ_c values found at 44 kHz. So, both curves do not represent fits to the experimental data points but are calculated curves.

We will first discuss the $T_{1\rho}(^{13}C)$ relaxation data of the ethylene carbons of the amorphous yarn (500) (see also Table 3). At ν_1 = 44 kHz only one relaxation time was observed (1.7 ms), and at ν_1 = 78 kHz two relaxation times (1.5 and 21.5 ms) were involved in the relaxation process. As indicated in Figure 8, this can be explained by assuming that the single $T_{1\rho}(^{13}C)$ observed at 44 kHz is caused by contributions from two independent motions with different τ_c's on both sides of the minimum (at $\tau_c \sim 5 \times 10^{-6}$ s). Consequently, the relaxation time corresponding to a short τ_c ($\omega_1\tau_c < 1$) shows no dependence on ν_1 (1.7 → 1.5 ms), whereas the relaxation time corresponding to the longer τ_c ($\omega_1\tau_c > 1$) changes from 1.7 to 21.5 ms. This brings us to the interesting conclusion that in the yarn which is almost completely amorphous according to X-ray measurements (V_C = 0.01; see Table 1) we distinguish a relatively fast and a relatively slow ethylene motion with a correlation time of $\tau_c < \sim 5 \times 10^{-6}$ s and $\tau_c > \sim 5 \times 10^{-6}$ s, respectively. This is in agreement with the observation of two $T_{1\rho}(^{13}C)$ relaxation times of protonated aromatic carbons for sample 500 (see Table 3), which points to the existence of relatively fast and slow aromatic ring motions in the amorphous yarn.

From the ν_1 dependence of the ethylene $T_{1\rho}(^{13}C)$ values of sample 5500(10%) (see Table 3), it is expected that both ethylene motions in this yarn correspond to correlation times of $\tau_c > \sim 5 \times 10^{-6}$ s.

From Table 3 it is apparent that both for the amorphous and for the semicrystalline sample (500 and 5500(10%)) the short relaxation time of the protonated aromatic carbon shows a less than $(\nu_1)^2$ dependence. This would indicate that these relaxation times correspond with correlation times around the $\omega_1\tau_c = 1$ minimum ($\tau_c \approx 5 \times 10^{-6}$ s).

Our conclusions are in general agreement with the results of other authors. For example, Ward[22] concluded from his ^{1}H NMR study of PET films that ethylene reorientation occurs at frequencies greater than 10^5 Hz and that aromatic rings undergo reorientations with similar frequencies. Sefcik et al.[5] also observed a small change in $\langle T_{1\rho}(^{13}C)\rangle$ of aromatic carbons with the applied ν_1 field, suggesting some phenyl reorientation at frequencies comparable to the applied ν_1 field (28–44 kHz).

C. $T_{1\rho}(^1H)$ Relaxation. The $T_{1\rho}(^1H)$ relaxation decay was monitored by measuring the decay of either ethylene, aromatic, or carbonyl carbon signal intensities. All of them showed identical decays. Apparently, spin diffusion[14-16,19] is effective enough to average the intrinsic $T_{1\rho}(^1H)$ relaxation times of chemically different protons, making interpretation of the data in terms of localized motions impossible. In order to increase the accuracy of the measurements, the experimental data at different τ are taken as the average signal intensities of different carbons.

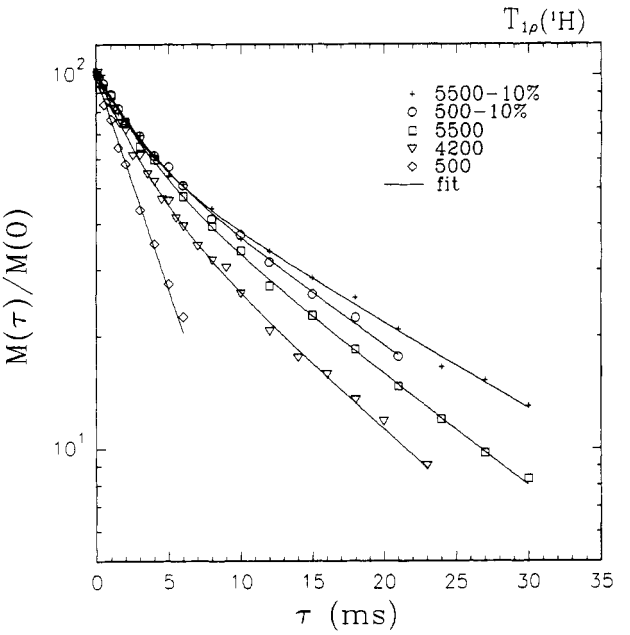

Figure 9. Decay of ^{1}H magnetization in the rotating frame (ν_1 = 44 kHz, rotor speed = 4.6 kHz) for the five different PET yarns. Solid lines represent least-squares fits to the relaxation data with one or two components using eq 1. Experimental data points represent averaged intensity values of ethylene, aroamtic, and carbonyl carbons.

Table 4. $T_{1\rho}(^1H)$ Relaxation Parameters with Dimensions $\langle x\rangle$ of Rigid Regions As Calculated from the Longer $T_{1\rho}(^1H)_B$ Values As Described in the Text[a]

sample	$T_{1\rho}(^1H)_A$ (ms)	$T_{1\rho}(^1H)_B$ (ms)	I_A (%)	I_B (%)	x (X-ray) (Å)	$\langle x\rangle$ (NMR) (Å)
1. 5500(10%)	3.0 ± 0.4	19.0 ± 1.3	39 ± 3.6	61 ± 3.9	101	106
2. 500(10%)	3.0 ± 0.6	15.8 ± 1.7	34 ± 6.7	66 ± 7.0	101	97
3. 5500	3.3 ± 0.4	14.7 ± 1.0	40 ± 4.8	60 ± 5.0	91	94
4. 4200	2.9 ± 0.4	12.8 ± 1.4	47 ± 7.0	53 ± 7.2	81	87
5. 500	3.8 ± 0.2		100 ± 1.7			<50

[a] The X-ray data represent the crystal lengths along the fiber axis.

The decay of ^{1}H magnetization of the five PET yarns is shown in Figure 9. This plot clearly indicates that the decay of all semicrystalline yarns involves at least two different $T_{1\rho}(^1H)$ relaxation times. Our observations are in agreement with the results of Cheung et al.,[8] who performed $T_{1\rho}(^1H)$ measurements on 50% crystalline PET samples. The decay of the amorphous sample could be fitted well with one exponential. The $T_{1\rho}(^1H)$ values of each sample are summarized in Table 4.

For the interpretation of the relaxation data we have to establish whether spin diffusion plays a role in our system. The effect of spin diffusion on the relaxation behavior of heterogeneous systems has been extensively studied by Packer and co-workers.[14,15] From their simulation studies of relaxation in the presence of spin diffusion, it became clear that different relaxation times cannot be simply interpreted in terms of different molecular motions within the sample. The relaxation behavior of a multiregion system depends on the rate of spin diffusion, on the difference in intrinsic relaxation times, and on the sizes of the regions relaxing at different rates.

The dimensions of the crystalline regions can be determined by X-ray measurements. The crystal lengths along the fiber axis, x(X-ray), vary from 81 to 101 Å (see Table 4). Calculations of the distance magnetization can travel within a time t by spin diffusion depend on the choice of model describing the physical structure. Reported values for the mean-square distance, $\langle x^2\rangle$, mag-

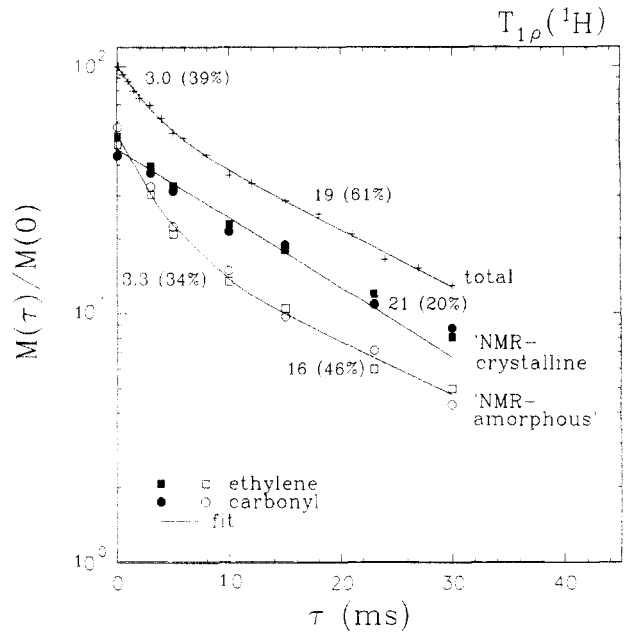

Figure 10. $T_{1\rho}(^1H)$ relaxation behavior of total resonance and individual NMR crystalline and NMR amorphous components of ethylene and carbonyl resonances of sample 5500(10%). $T_{1\rho}(^1H)$ relaxation times (in ms) with fractions (in brackets) corresponding to each slope are given in the same figure. Solid lines represent least-squares fits to the relaxation data using eq 1.

netization can travel within a time t vary between $^4/_3Dt$[7] and $2Dt$[14,24] for a one-dimensional model and $6Dt$ for a three-dimensional model.[25] Havens and VanderHart[7] reported a value for the spin diffusion coefficient (D) for PET of 5×10^{-12} cm^2/s. It should be noted that in a $T_{1\rho}(^1H)$ experiment, where spin diffusion occurs in the presence of an on-resonance radio-frequency field on protons, the spin diffusion coefficient is half the value of that in the laboratory frame.[7,25] When we assume that spin diffusion occurs in three dimensions, it can be calculated that for a two-region system with sizes of 100 Å, a steady-state diffusion profile over the entire sample will be established within approximately 15 ms. It is therefore reasonable to assume that the observed longer relaxation time reflects a spin diffusion time, i.e., the time magnetization needs to diffuse out of a region with a long relaxation time into a region with a shorter relaxation time, which acts as a relaxation sink. The interpretation of the long-time behavior of proton relaxation in the rotating frame in terms of a spin diffusion time has also been proposed by Packer et al.[14] based on their calculations and experimental results. Support for this assumption is given by the individual decays of magnetization in the NMR amorphous and NMR crystalline regions, as measured by spectral deconvolution as described before. The results are presented in Figure 10 for sample 5500(10%). This plot shows that the short relaxation time of 3.3 ms reflects the initial fast decay of the magnetization in the mobile NMR amorphous phase. At the final stage in the relaxation process, the NMR amorphous phase relaxes at approximately the same rate as the NMR crystalline phase.

A rough estimate of the sizes of the regions relaxing with intrinsically longer relaxation times can now be obtained by calculating $\langle x \rangle = (6Dt)^{1/2}$, where t is given by the longer relaxation time. These values are summarized in Table 4. Although these calculations depend strongly on the choice of model and the value of the diffusion coefficient, the calculated values seem to agree well with the X-ray data given in the same Table.

For the amorphous yarn (sample 500) only one single $T_{1\rho}(^1H)$ relaxation time is observed. However, two $T_{1\rho}(^{13}C)$ and two T_{CH} values were obtained for this sample, indicating different motions within this sample. Probably the sizes of regions with different mobilities are relatively small compared to the distance that can be bridged by spin diffusion. According to a relaxation time of 3.8 ms, these regions can be calculated to be smaller than 50 Å.

D. T_{CH}. Characteristic cross-polarization transfer times of magnetization from ^1H to ^{13}C, T_{CH}, have an r_{CH}^{-6} dependence, where r_{CH} is the distance between a ^{13}C and a ^1H nucleus. In addition, molecular motions can affect T_{CH} values, because they can effectively reduce ^1H–^{13}C dipolar interactions necessary for magnetization transfer.[9]

Typical cross-polarization curves for protonated (ethylene) and nonprotonated (carbonyl) carbons are shown in Figure 11a for sample 5500(10%). It is clear that the buildup of magnetization goes at a slower rate for carbonyl than for ethylene carbons, the latter having directly bonded protons. The decay of magnetization follows the $T_{1\rho}(^1H)$ relaxation behavior. In order to obtain accurate T_{CH} values, $T_{1\rho}(^1H)$ values were held fixed during data fitting at values determined separately in the $T_{1\rho}(^1H)$ experiment (see Table 4).

In Figure 11b it is shown that the buildup of the ethylene carbon magnetization can be decomposed into two exponential processes, with characteristic times of 0.018 and 0.22 ms. The dashed lines represent the individual components. A fit to the experimental data with one T_{CH} value, which is clearly worse than that with two components, is also shown.

Formally, a buildup time of 18 μs cannot be described by a T_{CH}, which implies thermal equilibrium within the proton spin system. The proton spin system reaches a thermal equilibrium state after a time on the order of the proton T_2. As long as a proton spin temperature is not defined, the magnetization buildup should be described as a transient phenomenon.[9] In the same way as for the cross-polarization time T_{CH}, the initial buildup of magnetization due to the transient phenomenon is inversely proportional to the heteronuclear van Vleck second moment, M_2^{IS}, which is a measure of the dipolar coupling between ^1H and ^{13}C spins.[9] So, for both transient and thermodynamic processes, short buildup times must correspond to rigid systems. Although at very short times τ, the transient process seems to be more reasonable, we use a loosely defined T_{CH} value to describe the initial buildup of magnetization. In principle, a similar problem exists for the carbon spin system, for which a spin temperature is defined only after a very long carbon-13 T_2.

From $T_{1\rho}(^{13}C)$ measurements, we would expect that three T_{CH} parameters are needed to fit the data. However, probably because of the limited number of data points, a three-component fit yielded the same fit as with two components. From the fitting results it appears that the component with the short T_{CH} value (0.018 ms) decays with the longer $T_{1\rho}(^1H)$ (19 ms) and the one with the longer T_{CH} value (0.22 ms) with the shorter $T_{1\rho}(^1H)$ (3 ms). This holds for all semicrystalline yarns, which proves that our assignment of the long $T_{1\rho}(^1H)$ to rigid domains and of the short $T_{1\rho}(^1H)$ to mobile domains is correct, because the short T_{CH} value must correspond to rigid regions. Table 5 summarizes the results. Two T_{CH} values for the ethylene and protonated aromatic carbons are obtained for the amorphous yarn, confirming the heterogeneity in molecular motion in this yarn as followed from $T_{1\rho}(^{13}C)$ measurements.

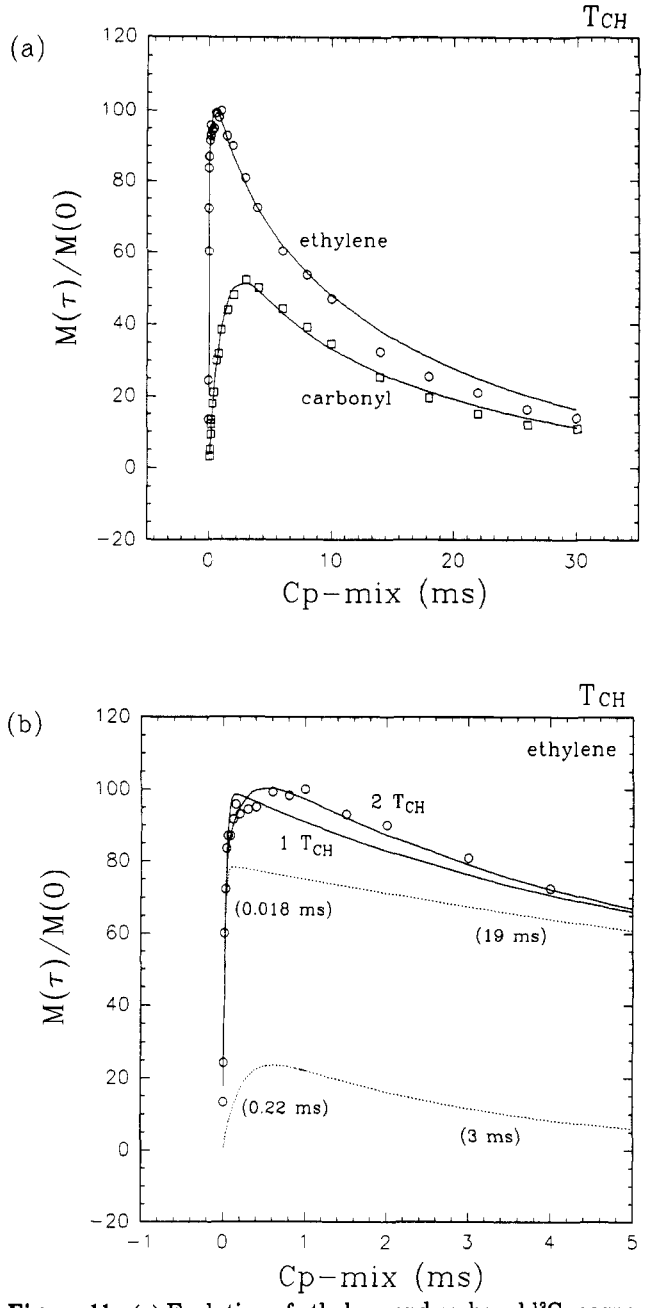

Figure 11. (a) Evolution of ethylene and carbonyl ^{13}C magnetization in a variable cross-polarization contact-time experiment of sample 5500(10%). Solid lines represent least-squares fits with eq (2). (b) Expanded plot of the buildup of ethylene carbon magnetization of sample 5500(10%), showing least-squares fits with eq (2) with one and two T_{CH} values. For the two-component fit the individual components are plotted (dashed lines) with characteristic time constants T_{CH} and $T_{1\rho}(^1H)$ (in brackets).

For all yarns, the buildup of the magnetization of nonprotonated aromatic and carbonyl carbons goes at a single rate. This means that the difference in molecular motion between mobile and rigid regions affecting T_{CH} values of protonated carbons apparently does not affect the T_{CH} values of nonprotonated carbons. We assume that this is due to the dominant effect of a large C–H distance for nonprotonated carbons yielding relatively long T_{CH} times.

At this point we point to a more general issue in interpreting relaxation parameters in terms of correlation time and amplitude of molecular motions. $T_{1\rho}(^{13}C)$ measurements reveal that in all samples there are at least two different types of motions: slow and fast motions relative to a correlation time of about 5×10^{-6} s. However, these conclusions are probably very much dependent on the motional model used, namely, a random isotropically rotating C–H pair. It is not clear how the relaxation time–correlation time dependence would look in the case of small-amplitude anisotropic motions. For the cross-polarization rates, T_{CH}^{-1}, this is different. Here the occurrence of a very short T_{CH} between 14 and 26 μs and a long T_{CH} between 340 and 1520 μs can only mean that in some parts of the yarns large-amplitude motions must exist which can average the angular part of the C–H dipolar interaction.

Information about the amplitude of aromatic ring molecular motions can be obtained by studying the principal elements of the chemical shift tensor of aromatic carbons as a function of temperature. Table 6 shows the tensor elements of the protonated and nonprotonated aromatic carbons of the semicrystalline sample 5500(10%) and the amorphous sample 500 at different temperatures. These values, determined from a Herzfeld and Berger analysis,[23] represent "overall values". So for the semicrystalline yarn they are the averages of crystalline and amorphous regions. Up to at least 327 K, the chemical shift tensor elements remain independent of temperature. This means that up to this temperature no molecular motions occur which can reduce the chemical shift anisotropy. Since T_{CH} measurements show that in some

Table 5. T_{CH} Values and Fractions of (1) Ethylene, (2) Protonated Aromatic, (3) Nonprotonated Aromatic, and (4) Carbonyl Carbons

sample	T_{CH_A} (ms)	T_{CH_B} (ms)	I_A (%)	I_B (%)
		1. Ethylene		
1. 5500(10%)	0.22 ± 0.06	0.018 ± 0.002	27 ± 4.5	73 ± 2.8
2. 500(10%)		0.021 ± 0.002		100 ± 2.5
3. 5500	0.10 ± 0.02	0.016 ± 0.002	35 ± 5.1	65 ± 3.7
4. 4200	0.09 ± 0.02	0.014 ± 0.002	37 ± 5.2	63 ± 3.8
5. 500	1.10 ± 0.42	0.017 ± 0.002	27 ± 7.0	73 ± 1.8
		2. Protonated Aromatic		
1. 5500(10%)	1.52 ± 0.30	0.026 ± 0.002	40 ± 5.5	60 ± 1.7
2. 500(10%)	0.51 ± 0.24	0.022 ± 0.002	19 ± 5.8	81 ± 3.1
3. 5500	0.34 ± 0.08	0.019 ± 0.003	40 ± 5.6	60 ± 3.5
4. 4200	0.59 ± 0.12	0.025 ± 0.001	29 ± 3.9	71 ± 1.9
5. 500	0.99 ± 0.24	0.019 ± 0.002	37 ± 3.7	63 ± 2.7

sample	T_{CH} (ms)	sample	T_{CH} (ms)
	3. Nonprotonated Aromatic		
1. 5500(10%)	0.47 ± 0.08	4. 4200	0.31 ± 0.02
2. 500(10%)	0.28 ± 0.03	5. 500	0.65 ± 0.10
3. 5500	0.49 ± 0.05		
	4. Carbonyl		
1. 5500(10%)	1.08 ± 0.10	4. 4200	0.88 ± 0.06
2. 500(10%)	0.76 ± 0.04	5. 500	1.07 ± 0.07
3. 5500	0.91 ± 0.05		

Table 6. Principal Values of the Chemical Shift Tensor of the Protonated and Nonprotonated Aromatic Carbons of Samples 5500(10%) and 500 Measured at Different Temperatures

	nonprotonated aromatic			protonated aromatic		
T (K)	σ_{11}	σ_{22}	σ_{33}	σ_{11}	σ_{22}	σ_{33}
			Sample 5500(10%)			
297	226	147	26	217	151	20
327	226	148	25	217	152	18
357	224	145	29	216	151	21
427	224	144	30	200	149	40
477	220	142	36	189	161	48
			Sample 500			
297	232	152	27	213	164	21
327	230	150	30	211	164	25
357	229	150	30	207	166	27
427	228	147	34	189	168	43
477	233	145	37	182	176	49

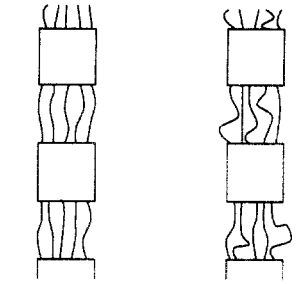

Figure 12. Schematic representation of different orientation distributions in the amorphous phase.

regions large-amplitude motions must exist, we assume that these parts (which constitute ~30% of the sample) may not fully contribute to the spinning sideband intensities, which are used for the determination of the chemical shift principal values of Table 6. In that case it follows from Table 6 that, in the rigid (crystalline) regions of both the semicrystalline and the amorphous yarn, phenyl reorientations must have a small amplitude (not exceeding ~5°), which do not change significantly with temperature. This aspect needs further investigation.

When comparing the T_{CH_A} values with crystallinity data (V_C) and F_{as} and F_{as}/F_{ab} data given in Table 1, it will be clear that there is no direct proportionality between T_{CH_A} values and one of these parameters. For instance, large differences in T_{CH_A} values are observed between samples 5500(10%) and 500(10%), while the crystallinity in both yarns is about the same (~35%). In fact, a longer T_{CH_A} value of ethylene carbons of sample 500(10%) is not observed. So we conclude that sample 5500(10%) contains more relatively disordered chains than sample 500(10%), giving rise to relatively large amplitude motions. More evidence for this point is obtained from F_{as} and F_{as}/F_{ab} data. The average orientation in the amorphous phase, indicated by F_{as} data, is relatively high for both drawn yarns (0.799 and 0.821; see Table 1). A larger contour-length distribution of sample 5500(10%), as indicated by F_{as}/F_{ab} values, means that besides highly ordered chains there are also less ordered chains in this yarn, while for sample 500(10%) all chains are more ordered to the same degree. This difference in contour-length distribution is graphically illustrated in Figure 12. We suppose that those chain loops or possibly chain ends in the amorphous phase of sample 5500(10%) undergo large-amplitude motions. So we find that the mobility in the amorphous phase of drawn yarns spun at high speeds is higher than that for drawn yarns spun at low speeds, although both spinning processes yield about the same crystallinity. Apparently, molecular motions are highly influenced by the processing history.

Summary and Conclusions

Three types of molecular motion were observed for semicrystalline PET yarns. These motions are assigned to different domains in the sample: a crystalline, a rigid amorphous, and a mobile amorphous region. In an amorphous yarn, two different types of molecular motion occur with correlation times shorter and longer than $\sim 5 \times 10^{-6}$ s. The regions which differ in molecular motion in the amorphous yarn have dimensions smaller than 50 Å, while the rigid and mobile domains in semicrystalline yarns are larger than 50 Å. For all yarns it is found that in the mobile amorphous regions aromatic rings and ethylene groups undergo large-amplitude motions. In crystalline regions and in the rigid parts of the amorphous yarn, phenyl reorientations have a very small amplitude (not exceeding ~5°). The mobility in the amorphous phase strongly depends on the process conditions. For instance, the mobility in the amorphous phase of a drawn semicrystalline yarn spun at a relatively high speed is higher than that in a drawn yarn spun at a relatively low speed.

Acknowledgment. We thank H. M. Heuvel and A. P. de Weijer for providing the X-ray and F_{as}/F_{ab} data of the series of PET yarns and for very helpful and stimulating discussions.

References and Notes

(1) Huisman, R.; Heuvel, H. M. *J. Appl. Polym. Sci.* **1989**, *37*, 595.
(2) Heuvel, H. M.; Huisman, R. *J. Appl. Polym. Sci.* **1978**, *22*, 2229.
(3) Schaefer, J.; Stejskal, E. O.; Steger, T. R.; Sefcik, M. D.; McKay, R. A. *Macromolecules* **1980**, *13*, 1121.
(4) Schaefer, J.; Stejskal, E. O.; Buchdahl, R. *Macromolecules* **1977**, *10* (2), 384.
(5) Sefcik, M. D.; Schaefer, J.; Stejskal, E. O.; McKay, R. A. *Macromolecules* **1980**, *13*, 1132.
(6) English, A. D. *Macromolecules* **1985**, *17*, 2182.
(7) Havens, J. R.; VanderHart, D. L. *Macromolecules* **1985**, *18*, 1663.
(8) Cheung, T. T. P.; Gerstein, B. C.; Ryan, L. M.; Taylor, R. E.; Dybowsky, D. R. *J. Chem. Phys.* **1980**, *73* (12), 6059.
(9) Demco, D. E.; Tegenfeldt, J.; Waugh, J. S. *Phys. Rev. B* **1975**, *11*, 4133.
(10) Stejskal, E. O.; Schaefer, J. *J. Magn. Reson.* **1975**, *18*, 560.
(11) Stejskal, E. O.; Schaefer, J.; Sefcik, M. D.; McKay, R. A. *Macromolecules* **1981**, *14*, 275.
(12) Huisman, R.; Heuvel, H. M. *J. Appl. Polym. Sci.* **1978**, *22*, 943.
(13) Komoroski, R. A., *Macromolecules* **1984**, *17*, 2182.
(14) Packer, K. J.; Pope, J. M.; Yeung, R. R.; Cudby, M. E. A. *J. Polym. Sci.* **1984**, *22*, 589.
(15) Kenwright, A. M.; Packer, K. J.; Say, B. J. *J. Magn. Reson.* **1986**, *69*, 426.
(16) VanderHart, D. L.; Garroway, A. N. *J. Chem. Phys.* **1979**, *71* (7), 2773.
(17) Garroway, N. *J. Magn. Reson.* **1979**, *34*, 283.
(18) Heuvel, H. M.; Lucas, L. J.; van den Heuvel, C. J. M.; De Weijer, A. P. *J. Appl. Polym. Sci.* **1992**, *45*, 1649.
(19) Packer, K. J.; Poplett, I. J. F.; Taylor, M. J. *J. Chem. Soc., Faraday Trans. 1* **1988**, *84* (11), 3851.
(20) Komoroski, R. A. *High Resolution NMR spectroscopy of synthetic polymers in bulk*, **1986**, 103–106.
(21) Tzou, D. L.; Desai, P.; Abhiraman, A. S.; Huang, T. H. *J. Polym. Sci.* **1991**, *29*, 49.
(22) Ward, I. M. *Trans. Faraday Soc.* **1960**, *56*, 648.
(23) Herzfeld, J.; Berger, A. E. *J. Chem. Phys.* **1980**, *73*, 6021.
(24) Cheung, T. T. P.; Gerstein, B. C. *J. Appl. Phys.* **1981**, *52* (9), 5517.
(25) Henrichs, P. M.; Tribone, J.; Massa, D. J.; Hewitt, J. M. *Macromolecules* **1988**, *21*, 1282.